Journal of Physics D: Applied Physics

PAPER

Reconfigurable RF notch filter based on an integrated silicon optical true time delay line

To cite this article: Jiayu Jing *et al* 2019 *J. Phys. D: Appl. Phys.* **52** 194001

IOP Publishing Journal of Physics D: Applied Physics
J. Phys. D: Appl. Phys. **52** (2019) 194001 (9pp) https://doi.org/10.1088/1361-6463/ab0735

Reconfigurable RF notch filter based on an integrated silicon optical true time delay line

Jiayu Jing[1], Xinyi Wang[1], Liangjun Lu[1], Linjie Zhou[1], Haowen Shu[2], Xingjun Wang[2] and Jianping Chen[1]

[1] State Key Laboratory of Advanced Optical Communication Systems and Networks, Department of Electronic Engineering, Shanghai Jiao Tong University, Shanghai 200240, People's Republic of China
[2] State Key Laboratory of Advanced Optical Communication Systems and Networks, School of Electronics Engineering and Computer Science, Peking University, Beijing 100871, People's Republic of China

E-mail: ljzhou@sjtu.edu.cn

Received 9 November 2018, revised 28 January 2019
Accepted for publication 14 February 2019
Published 1 March 2019

Abstract

The development of radio-frequency (RF) filters with bandwidth reconfigurability and frequency tunability in the MHz range is increasingly important to broadband wireless communication and radar systems. In this paper, we demonstrate a reconfigurable RF filter based on a silicon integrated optical true time delay line (OTTDL). The OTTDL is a four-path parallel structure with the reconfiguration enabled by thermo-optic Mach–Zehnder interferometer switches. By controlling the power splitting ratio of the switches, three different orders of finite impulse response filters with a variable bandwidth are realized. The bandwidth can be varied from 180.9 MHz to 662.0 MHz and the center frequency can be tuned in one free-spectral range up to 1 GHz.

Keywords: silicon photonics, optical delay line, RF filter, microwave photonics

(Some figures may appear in colour only in the online journal)

1. Introduction

Microwave photonics (MWP) technology, which has been an increasingly focused research field in recent years [1–3], has multiple advantages including broad bandwidth, low power consumption, high reconfigurability, and immunity to electromagnetic interference (EMI) [4]. The microwave signal can be transported and processed in the optical domain, breaking through the bottleneck caused by the limited speed of electrical systems [5]. One of the basic devices in MWP technologies is the microwave photonic filter (MPF), which has a broader processing bandwidth than the electrical filters [6]. MPFs can be divided into coherent and incoherent filters [4]. They can find rich applications in various devices and systems, for example, sensors [7, 8], optoelectronic oscillators (OEOs) [9], arbitrary microwave waveform generation and pulse compression [10], and multi-beamforming [11] etc. The notch filter, which is a kind of coherent filter, is also an essential part in radar systems, broadband wireless networks, and satellite communications [12, 13], because it can remove undesired interference signals in the systems [14].

Multiple MPFs demonstrated in the literature are made up of discrete components, such as frequency-to-time mapping based fiber delay lines [15], fiber Bragg gratings (FBGs) [16], and few mode fibers (FMFs) [17]. These fiber components are bulky and suffering from potential stability issues. The MFPs made of integrated photonic circuits are much compact [18], which can be implemented on various platforms such as III–V semiconductors [19], silicon photonics [20], Si_3N_4/SiO_2 planar lightwave circuits [21], and hybrid photonic integration circuits [22]. There are many mechanisms and optical structures that can be employed to realize integrated MPFs, such as stimulated Brillouin scattering [23, 24], optical delay lines (ODLs) [25], waveguide Bragg gratings [26], semiconductor

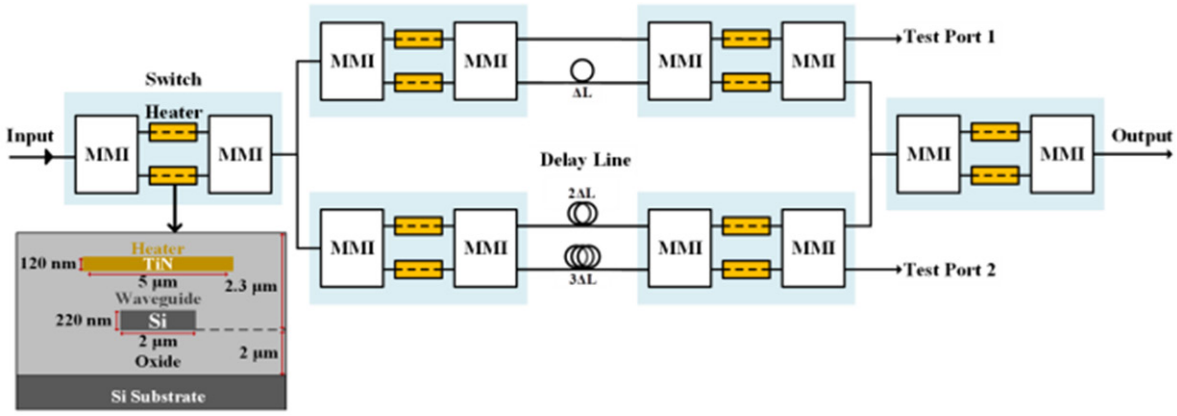

Figure 1. Schematic structure of the optical filter based on a four-path parallel optical delay line. The inset shows the cross-sectional view of the waveguide tuned by a TiN microheater on top.

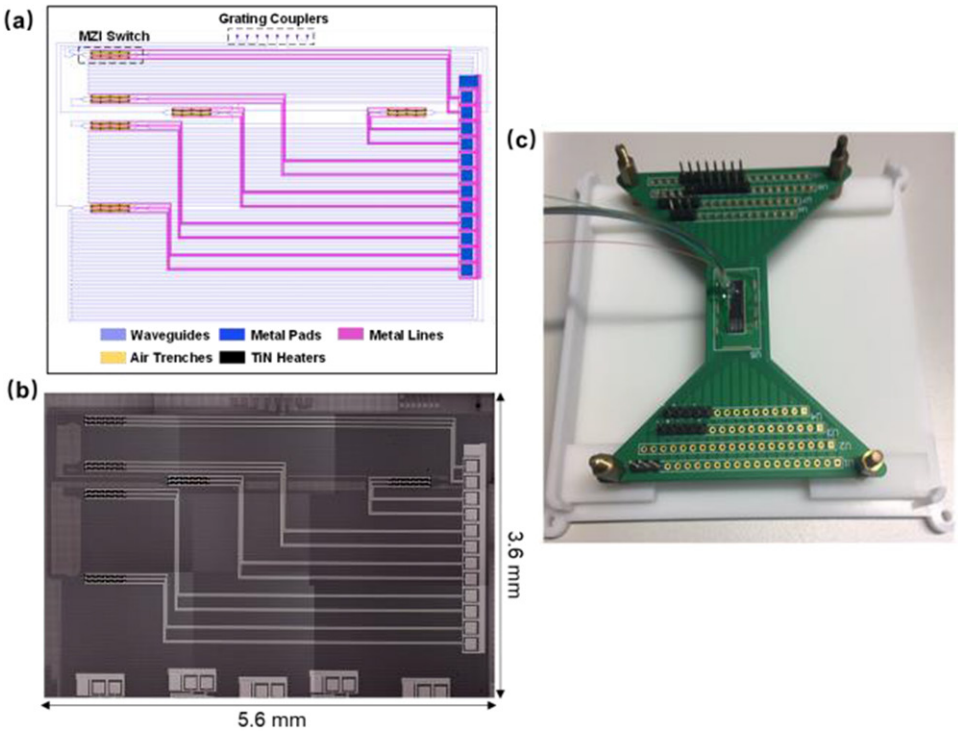

Figure 2. (a) Chip mask layout of the four-path parallel optical delay line. (b) Microscope image of the fabricated chip. (c) Photo of the home-packaged chip with fiber array coupling and wire bonding.

optical amplifiers [27], and ring resonators [28]. In [29], a microwave photonic notch filter based on a silica microsphere cavity is demonstrated. The bandwidth of the filter is fixed at about 2.2 MHz determined by the Q-factor the microsphehtere resonator. The filter center frequency can be tuned by over 15 GHz. In recent years, silicon photonics has attracted great interest because of its compactness, low cost, and compatibility with CMOS technologies. A 4-tap ODL-based finite impulse response (FIR) filter has been demonstrated on the silicon photonics platform [30], but the bandwidth of the filter is too large (>20 GHz), which is not suitable for high-resolution RF applications. However, the tunability of bandwidth is not available along the whole tuning range. In our work, we demonstrate a more flexible microwave photonic notch filter. The bandwidth of MPF can be tuned along the center frequency tuning range.

In this work, we experimentally demonstrate a 4-tap FIR RF notch filter based on the silicon integrated optical true time delay line (OTTDL). The filter center frequency can be tuned in one free-spectral range (FSR) up to 1 GHz. The filter can be reconfigured to three different orders, allowing the bandwidth to be tuned from 180.9 MHz to 662.0 MHz. The extinction ratio of the notch filter is larger than 20 dB for all configurations. Compared to other photonic-based approaches, our device has the merits of more flexible bandwidth tunability (compared to [29]), higher resolution (compared to [30]), and more compact (compared to [15–17]). The RF filters made of pure electrical components usually have a limited tuning range in both center frequency and bandwidth [31–33]. For example, in [31], the RF filter has a frequency tuning range of 1.1–2.7 GHz and the bandwidth can be tuned in the ranges of 26–126 MHz and 24–200 MHz for two frequencies of

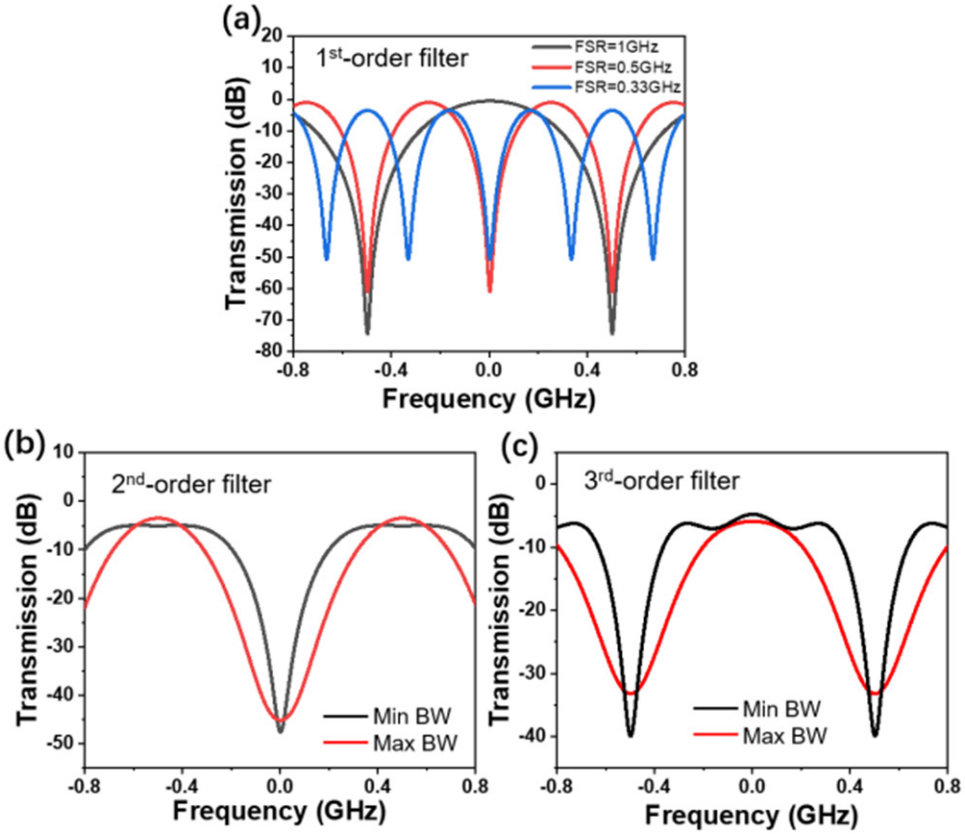

Figure 3. Simulation results of the optical FIR notch filter. (a) First-order optical filter with FSR = 1 GHz, 0.5 GHz and 0.33 GHz. (b) Second-order optical filter. (c) Third-order optical filter.

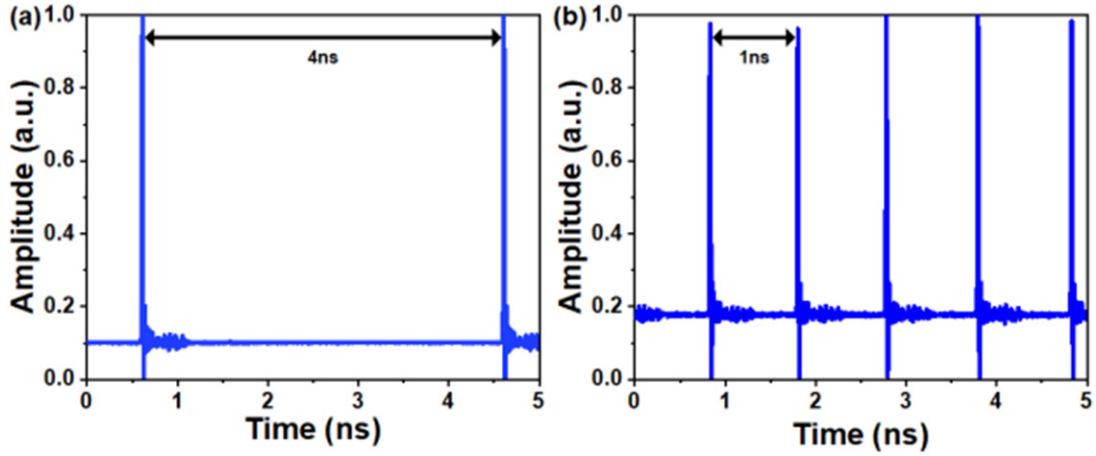

Figure 4. Measured optical waveforms of (a) 250 MHz input optical pulse train and (b) 1 GHz output optical pulse train.

1.6 GHz and 2.0 GHz, respectively. Therefore, our RF photonic filters provide a larger tunable bandwidth and more flexibility in controlling the filter order.

2. Device design and fabrication

Figure 1 shows the schematic structure of the four-tap FIR filter based on a four-path parallel optical delay line. The input light is first divided into four paths by three 1 × 2 Mach–Zehnder interferometer (MZI) switches. The MZI switch is composed of two multimode interferometers (MMIs) connected by two arm waveguides with equal lengths. The delay difference between the adjacent delay lines is designed to be 1 ns. The four paths are then combined by two 2 × 2 MZI switches and a 2 × 1 MZI switch. Upon controlling the states of the switches, the number of paths that the light passes through can be set, thus changing the order of the FIR filter.

The test ports from the 2 × 2 switches are used to monitor the spectra of the top and bottom interference paths. The inset of figure 1 illustrates the cross-section of the thermo-optic (TO) phase shifter based on a TiN microheater. The silicon waveguide is of normally 500 nm width and 220 nm height for single-mode propagation. While in the long delay line and phase shift sections, it is tapered up to 2 μm wide in order to

reduce the propagation loss. Upon changing the splitting ratio of the switches, the FIR filter can be reconfigured to different notch profiles.

Figure 2(a) shows the mask layout of the optical filter. The input, output, and test ports are all terminated with grating couplers in an array so that a fiber array can be used for input/output coupling. The grating couplers have a pitch of 127 μm. The TiN-based phase shifters are connected with aluminum wires to electrical pads along the edge of the chip.

The chip was fabricated using CMOS-compatible fabrication processes on a silicon-on-insulator (SOI) wafer with a top silicon layer thickness of 220 nm and a buried oxide (BOE) layer thickness of 2 μm. The waveguides were patterned by deep ultraviolet (DUV) photolithography and transferred to the silicon layer by plasma dry etching. A 1.5 μm-thick silicon dioxide layer was deposited using chemical vapor deposition (CVD) on top of the waveguides as the upper cladding. Then a TiN layer with a thickness of 120 nm was sputtered and patterned as the microheater, followed by deposition of another silicon dioxide layer with a thickness of 0.8 μm. After that, contact holes were etched and aluminum electrical connections were formed by sputtering and dry etching. Finally, deep air trench was etched around the phase shifters to reduce thermal crosstalk and meanwhile increase thermal tuning efficiency. Figure 2(b) shows the microscope image of the chip. The chip size is 5.6 mm $\times$ 3.6 mm. Figure 2(c) shows the home-packaged chip. A fiber array was attached to the chip for optical coupling. The chip was wire-bonded to a printed circuit board (PCB) so that voltages can be applied to the chip.

3. Theory and simulation

As the optical filter is based on an OTTDL, the time-domain transfer function of the filter can be written as:

$$h(t) = \sum_{n=0}^{3} A_n \delta(t - nT) \tag{1}$$

where T is the delay resolution (1 ns in our design) and A_n is the amplitude of the optical field through an optical path adjustable by the MZI switches. After Fourier-transform of the transfer function from the time domain into the frequency domain, it can be written as:

$$H(\omega) = \sum_{n=0}^{3} A_n e^{-jn\omega T}. \tag{2}$$

The FIR filter can be reconfigured by changing the splitting ratio of the MZI switches. To realize the first-order filter, light only passes two paths, for example, the first and second paths ($A_2 = A_3 = 0$). The entire structure then becomes an unbalanced MZI, generating an interference spectrum with a free spectral range (FSR) of 1/T. Since the delay difference T is designed as 1 ns, the FSR is thus 1 GHz. Similarly, when light passes the first and the third paths ($A_1 = A_3 = 0$), an interference spectrum with a reduced FSR of 1/(2T) = 0.5 GHz is produced. When light passes the first and the fourth paths

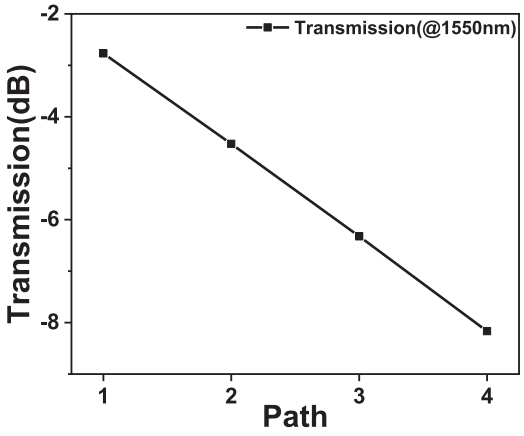

Figure 5. Normalized optical transmission of each path in the OTTDL.

($A_1 = A_2 = 0$), the FSR of the interference spectrum shrinks to $1/(3T) = 0.33$ GHz. Figure 3(a) shows the simulation result of the first-order filter. The notch 3 dB bandwidths are 659 MHz, 330 MHz, and 219 MHz, following the reduction of the FSR.

When it is reconfigured to the second-order filter, the first, second and third optical paths can be selected ($A_3 = 0$). The bandwidth of the spectrum can be adjusted by tuning A_0, A_1, and A_2. Figure 3(b) shows the spectra with the filter bandwidth changing from 365 MHz to 664 MHz. The corresponding A_n is [0.8, 0.8, 0.09, 0] for the minimum bandwidth and [0.74, 0.74, 0.1, 0] for the maximum bandwidth.

The third-order filter is implemented by selecting all four paths in the structure. The bandwidth can be adjusted from 228 MHz to 639.1 MHz, as seen from figure 3(c). The corresponding A_n is [0.19, 0.18, 0.75, 0.71] and [0.03, 0.03, 0.76, 0.74] to get the minimum and maximum bandwidths, respectively. The bandwidth tuning range is limited by the ripples presented in the passbands of the second and third-order filters. The ripple magnitude is set to be smaller than 3 dB as a criterion during the filter bandwidth tuning process.

4. Experiment and discussion

We first characterized the time division multiplexing performance of the OTTDL chip by setting the splitting ratio of all MZI switches to 50:50. The MZIs were tuned using external voltage sources with a resolution of 1 mV. Figure 4 shows the time domain optical waveforms for the input and output pulse trains. We used a mode-locked laser (MLL) (Onefive, Origami) to generate the input optical pulses with a repetition rate of 250 MHz. The light was tuned to transverse electric (TE) polarization by a polarization controller before coupled into the chip. The output light from the chip was amplified by an erbium doped fiber amplifier (EDFA) (Amonics, AEDFA-23-B-FA) and finally detected by a photodetector with a bandwidth of 40 GHz (Discovery Semiconductors, DSC10H) and measured by a sampling oscilloscope (Keysight, DAC-X 86100D). The output waveform shows an optical pulse train with time intervals of 0.9692 ns, 0.9790 ns, 1.0132 ns, and 1.0352 ns. The slight deviation from the targeted 1 ns is

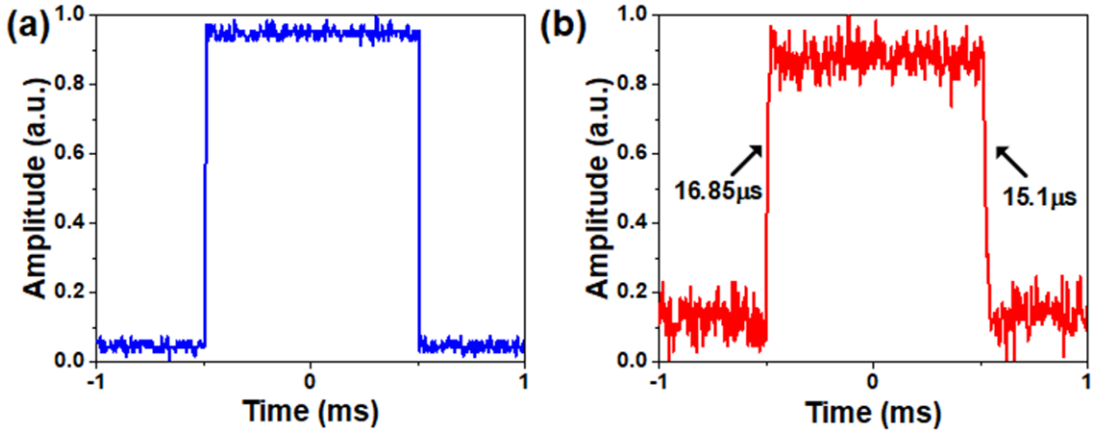

Figure 6. (a) Electrical pulse generated by a pulse generator. (b) Measured optical waveform of the switch.

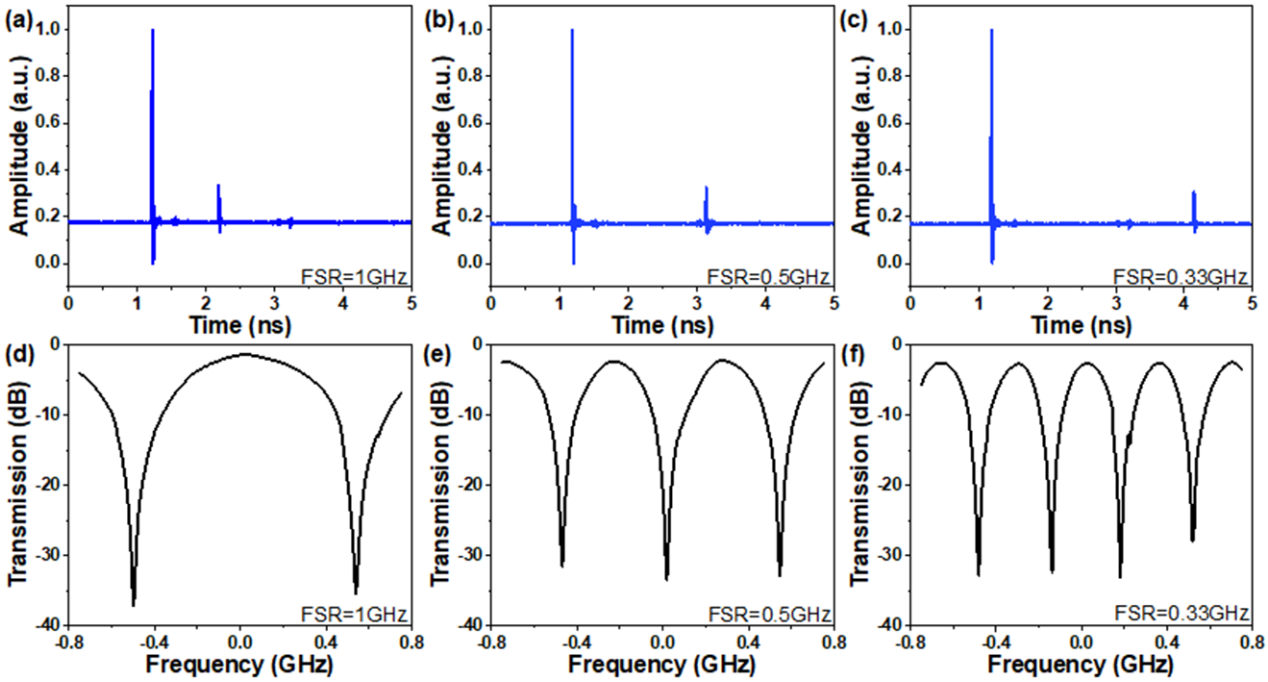

Figure 7. Measured time-domain and frequency-domain responses of the first-order optical notch filter. (a), (d) Time delay 1 ns; (b), (e) time delay 2 ns; (c), (f) time delay 3 ns.

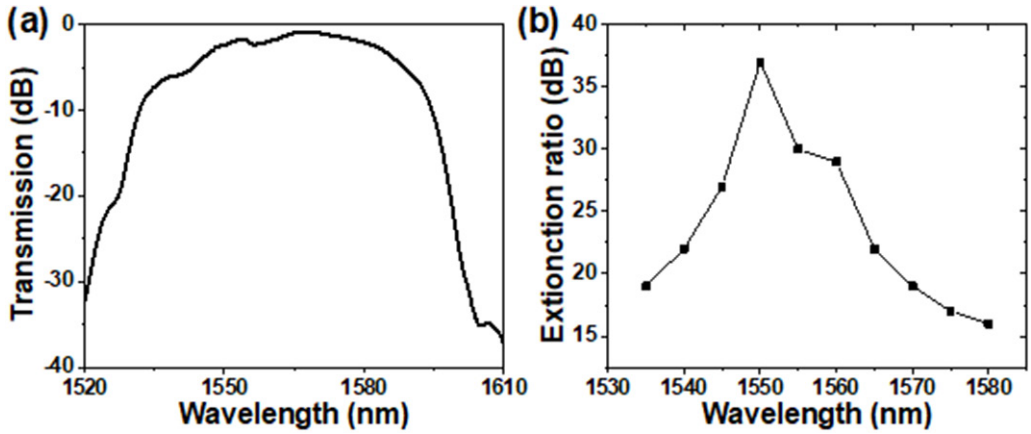

Figure 8. (a) Optical spectrum of the input 37.5 MHz MLL. (b) Extinction ratio change as a function of wavelength for the first-order FIR filter with 1 GHz FSR. The extinction ratio is a mean value within a 1 nm wavelength range.

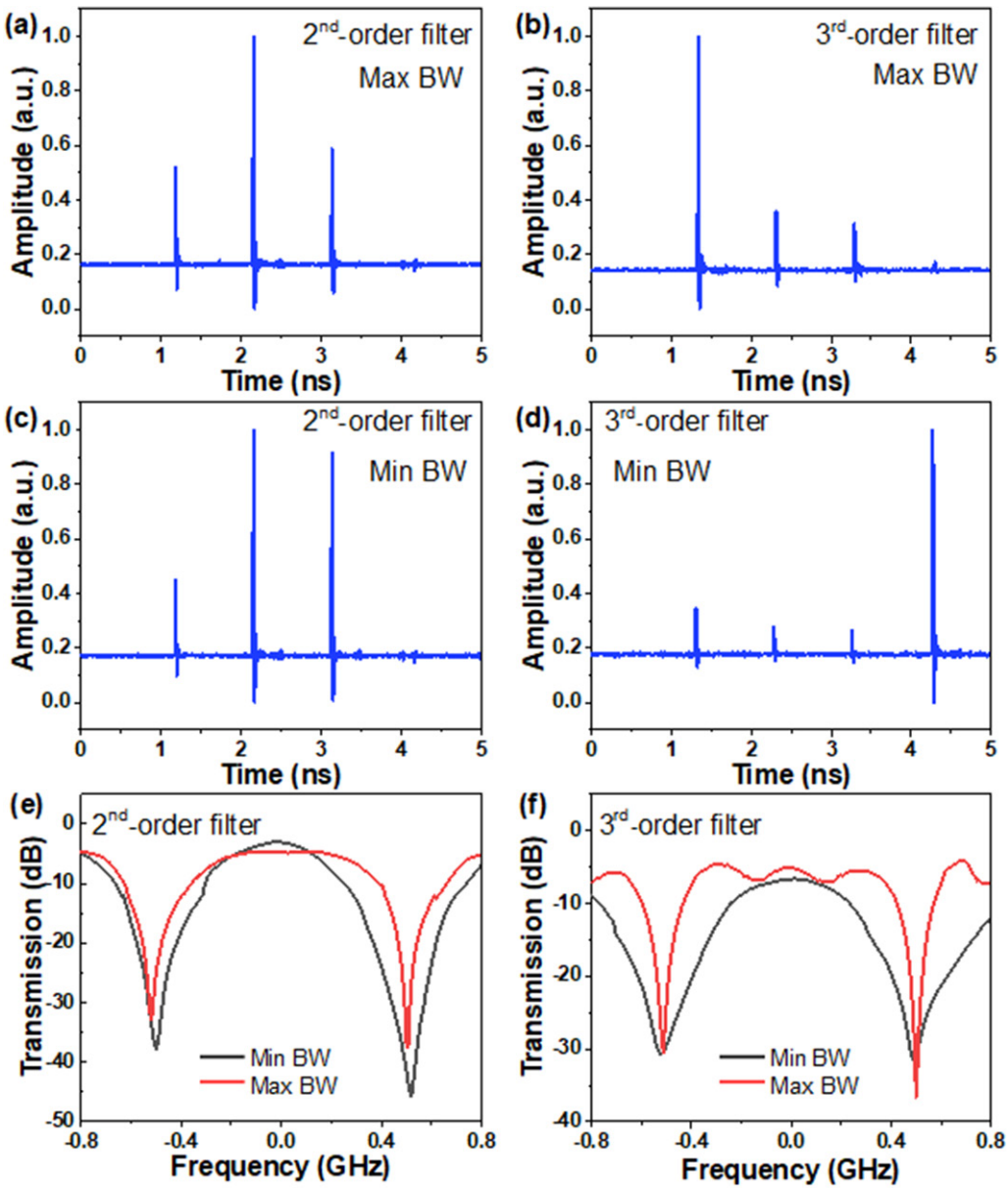

Figure 9. Measured time-domain and frequency-domain responses of the second-order (left column) and the third-order (right column) optical filters. (a), (b) Optical pulses responses at the maximum notch bandwidth; (c), (d) optical pulses responses at the minimum notch bandwidth; (e), (f) output transmission spectra.

probably due to the nonuniformity of the silicon waveguide layer and the fabrication errors that change the waveguide width. It should be noted that the tail of the pulse is caused by the photodetector due to its limited bandwidth.

Figure 5 shows the normalized on-chip transmission of each path in the delay line at the 1550 nm wavelength. The loss of each path is 2.77 dB, 4.53 dB, 6.32 dB and 8.17 dB. From the linear fitting, the average waveguide propagation loss is obtained to be around 0.25 dB cm^{-1}. It should be noted that the 500 nm-wide waveguide has a much higher loss of around 2.5 dB cm^{-1}. Thus, it reveals that widening waveguide in long straight sections is an effective method to reduce the overall loss.

The characterization of the MZI switch indicates that it has a large operating bandwidth over 80 nm and the static switching extinction ratio is about 25 dB. The power consumption to change the switch from the cross-state to the bar-state is 26.4 mW, which can be reduced by etching off the silicon substrate underneath the microheater. We obtained the switching speed of the MZI switch by measuring the optical waveform when an electrical pulse was applied onto one arm of the MZI. Figure 6(a) shows the electrical pulse generated by a pulse generator (HP, 8131A). Figure 6(b) shows the time domain response of the optical switch. The measured rise-time and fall-time are 16.85 μs and 15.1 μs, respectively.

We also measured the optical pulse responses and the corresponding optical transmission spectra of the first-order FIR filter with three different FSRs, as shown in figure 7. The MLL (Precision Photonics, FFL1560) used in this measurement has a repetition rate of 37.5 MHz. The transmission spectrum was measured by wavelength scanning of a tunable laser (Santec, TSL-710) with a resolution of 0.05 pm. The notch extinction ratio is more than 30 dB due to the nearly

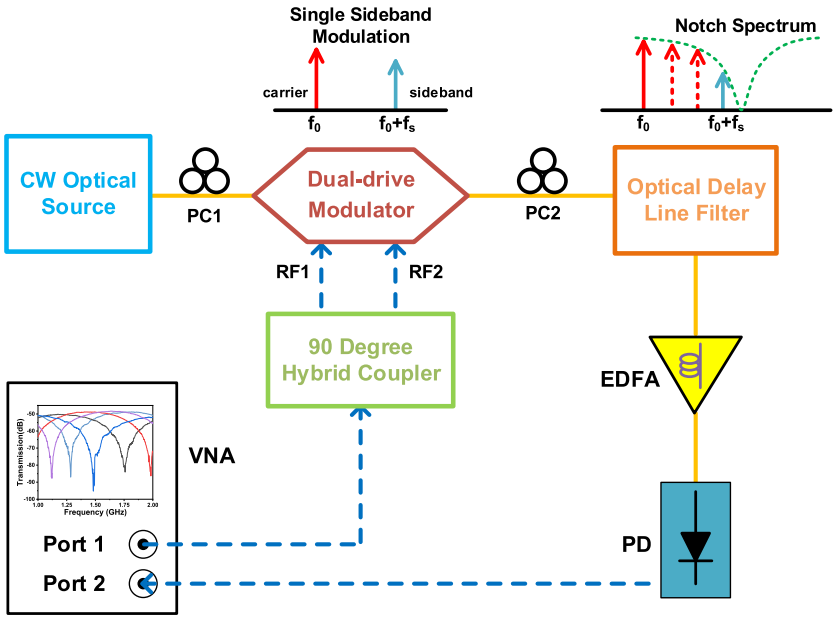

Figure 10. Experiment setup for the tunable RF filter. CW laser: continuous-wave tunable laser; PC: polarization controller; EDFA: erbium doped fiber amplifier; PD: photodetector; VNA: vector network analyzer.

balanced interference of the two optical paths at the measured wavelength of 1550 nm. The relative optical power of the pulses is [0.83, 0.17, 0, 0], [0.83, 0, 0.16, 0] and [0.83, 0, 0, 0.14] for the three cases.

Note that the optical pulse power is unequal even in the balanced interference. This is because the spectrum of the optical pulse from the MLL covers a broad wavelength range in which the splitting ratio of the MZIs varies significantly. Therefore, the balanced interference is only achieved around the target 1550 nm wavelength. Figure 8(a) shows the measured optical spectrum of the MLL, exhibiting a broad bandwidth of 10's nm. In this broad wavelength range, the notch extinction ratio changes considerably, as can be seen from figure 8(b). Thus, it implies that the MZI switches are wavelength dependent. To lower the wavelength sensitivity, MZI switches based on broadband couplers could be used [34].

Figure 9 illustrates the output optical pulses and the corresponding spectra of the second- and third-order optical notch filters when they are configured to provide the minimum and the maximum optical bandwidths. The bandwidth tuning range of the second-order filter is from 362.5 MHz to 662.5 MHz. The extinction ratio is larger than 30 dB. The output optical pulse power are [0.35, 0.83, 0.42, 0] and [0.28, 0.83, 0.75, 0] for the minimum and the maximum bandwidths, respectively. When the structure is reconfigured to the third-order filter, the bandwidth tuning range is from 234.4 MHz to 625 MHz. The optical pulse power is [0.86, 0.22, 0.18, 0.03] for the maximum bandwidth and [0.21, 0.14, 0.13, 0.86] for minimum bandwidth. The power consumption is 204.9 mW, 177.1 mW, and 200.8 mW for the first-order filter with an FSR of 1 GHz, 0.5 GHz, and 0.33 GHz, respectively. When it comes to second-order filter, the power consumption is 217.5 mW for the maximum bandwidth and 195.227 mW for the minimum bandwidth. The power consumption of the third-order filter is 213 mW and 236.1 mW for the maximum and the minimum bandwidths, respectively.

Figure 10 shows the experimental setup to realize the reconfigurable RF filter. The CW laser light (carrier frequency f_0) after the PC was modulated by a dual-parallel electro-optic modulator (Sumitomo, T.DKH1.5-10PD-ADC). The modulator was driven by two RF signals (modulation frequency f_s) with a 90° phase difference to realize the single sideband modulation. The orthogonal RF signals were generated from the vector network analyzer (VNA, Keysight, N5247A) followed by a 90° hybrid coupler (Krytar, Model 1831). The modulated light with two tones at f_0 and $f_0 + f_s$ went through another PC before coupling into the optical filter chip. The sideband tone at $f_0 + f_s$ was suppressed by the optical notch filter with the attenuation dependent on the relative position of the notch. The processed optical signal from the chip was amplified by an EDFA to compensate for the insertion loss of the chip and detected by a PD to implement the optical-to-electrical conversion. The RF signal was finally received by the VNA. The beating of the two frequency tones in the PD regenerated the RF signal with a notch spectrum mapped from the optical domain to the RF domain. The center frequency of the RF notch filter can be tuned either by shifting the optical notch wavelength or the laser wavelength. When the laser wavelength or the optical notch wavelength is shifted, the relative position between them is changed. As seen from the operation principle, the center frequency of the RF filter is thus tuned. It should be noted that our method to generate the RF filter is limited to the use of single sideband modulation. In [35], the implementation of a tunable RF notch filter uses double sideband modulation and two ring resonators have to be used to eliminate the double sidebands. It hence increases

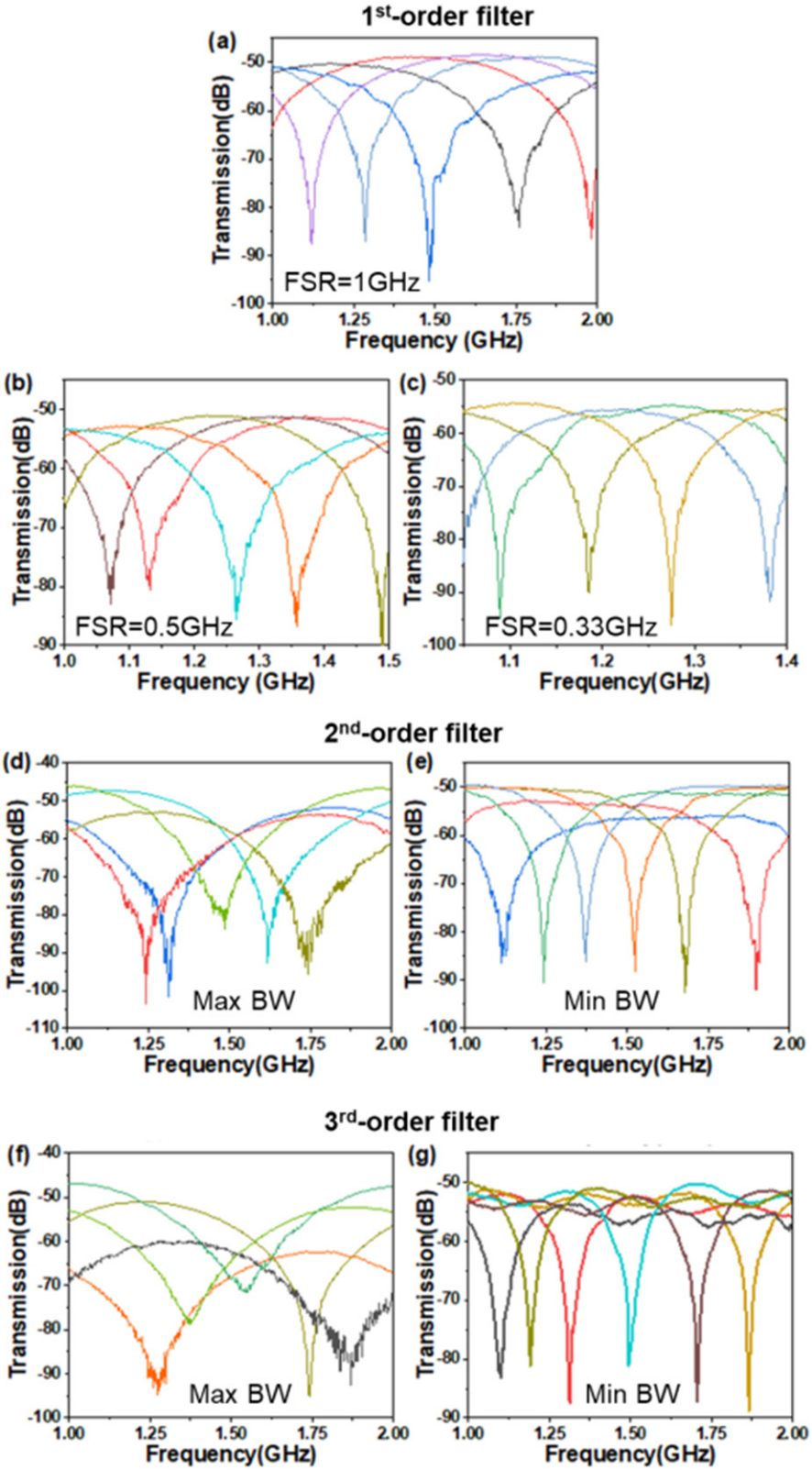

Figure 11. Measured RF spectra when the center frequency is tuned for the device configured as (a)–(c) first-order, (d), (e) second-order, and (f), (g) third-order filters. In the first-order filter, the FSR is changed from (a) 1 GHz, (b) 0.5 GHz, to (c) 0.33 GHz. In the second-order and third-order filters, the notch bandwidth varies from (d), (f) the maximum to (e), (g) the minimum.

the size and power consumption of the device. In [25], an multi-tap RF filter is synthesized based on a dispersive photonic crystal delay line. Its performance is affected by the power fading effect because the double-sideband modulation is employed.

Figure 11 shows the measured RF spectra when the optical filter is reconfigured to various orders. The measured frequency range covers one FSR of the filter, starting from 1 GHz because the 90° hybrid that we used only works beyond 1 GHz. The center frequency of the RF filter is tuned within one FSR by changing the laser wavelength.

The spectral profiles of the RF filter generally follow that of the optical filter. The notch extinction ratios are in between 30 dB to 40 dB. The notch bandwidth of the first-order RF filter is 428.6 MHz, 248.2 MHz, and 180.9 MHz when the FSR is 1 GHz, 0.5 GHz, and 0.33 GHz, respectively. The bandwidth of the second-order and third-order RF filters can be tuned from 356.8 MHz to 662.0 MHz and from 234.4 MHz to 612.5 MHz, respectively. It is consistent with the corresponding optical filters. One may notice that the RF power reduces when the RF filter center frequency is tuned close to the edge of one FSR, most notably for the broadband notch filters (see figures 11(d) and (f)). This is because the optical carrier is also highly attenuated when it falls in the valley of the optical notch spectrum when they are close enough. It should be noted that when the bandwidth of the filter is tuned close to or larger than 50% of the FSR, such as in the case of the first-order filter and the large-bandwidth second-order and third-order filters, the transmitted RF signal may be degraded because of the notches caused by the periodic performance of the optical filter.

5. Summary

We have demonstrated a reconfigurable FIR RF filter based on an integrated OTTDL. The OTTDL is made up of 4 parallel optical paths with a delay difference of around 1 ns. The RF filter was realized by beating the optical carrier and the single-sideband in a photodiode after they are processed by the OTTDL. Three orders of RF notch filters with a variable bandwidth have been implemented by selecting different optical paths with appropriate power ratios. The experimental results showed that the filter center frequency can be tuned to cover one FSR and the bandwidth can be tuned from 180.9 MHz to 662.0 MHz. Due to its narrow optical bandwidth, the RF filter can find rich applications in broadband wireless access networks and high-resolution radar systems.

Funding

This work was partially supported by the National Natural Science Foundation of China (NSFC) (61705129, 61535006) and Shanghai Municipal Science and Technology Major Project (2017SHZDZX03).

ORCID iDs

Jiayu Jing https://orcid.org/0000-0002-5831-8930

References

[1] Capmany J and Novak D 2017 *Nat. Photon.* **1** 319
[2] Chen L R 2017 *J. Lightwave Technol.* **4** 824
[3] Zhang W and Yao J 2016 *IEEE J. Quantum Electron.* **52** 0600412
[4] Capmany J, Ortega B and Pastor D 2006 *J. Lightwave Technol.* **24** 201
[5] Minasian R A 2006 *IEEE Trans. Microw. Theory Tech.* **2** 832
[6] Long J *et al* 2011 *IEEE Microw. Wirel. Compon. Lett.* **21** 74
[7] Xu O *et al* 2016 *Opt. Lett.* **41** 4859
[8] Liu J *et al* 2018 *J. Lightwave Technol.* **36** 4099
[9] Jiang F *et al* 2013 *Opt. Express* **21** 16381
[10] Zhang J and Yao J 2016 *J. Lightwave Technol.* **34** 5610
[11] Ye X *et al* 2015 *Opt. Express* **23** 10002
[12] Capmany J *et al* 2013 *J. Lightwave Technol.* **31** 571
[13] Yao J 2009 *J. Lightwave Technol.* **27** 314
[14] Gao Y *et al* 2018 *J. Lightwave Technol.* **36** 2152
[15] Mokhtari A *et al* 2013 *Opt. Express* **21** 21702
[16] Han X and Yao J 2015 *J. Lightwave Technol.* **33** 5133
[17] Nickel D V *et al* 2017 *J. Lightwave Technol.* **35** 5230
[18] Marpaung D *et al* 2013 *Laser Photonics Rev.* **7** 506
[19] Guzzon R S *et al* 2011 *Opt. Express* **19** 7816
[20] Lloret J *et al* 2011 *Opt. Express* **19** 12402
[21] Roeloffzen C G H *et al* 2013 *Opt. Express* **21** 22937
[22] Morrison B *et al* 2017 *Optica* **4** 847
[23] Byrnes A *et al* 2012 *Opt. Express* **20** 18836
[24] Marpaung D *et al* 2015 *Optica* **2** 76
[25] Sancho Durá J *et al* 2012 *Nat. Commun.* **3** 1075
[26] Burla M *et al* 2013 *Opt. Express* **21** 25120
[27] Jiang F *et al* 2016 *Opt. Express* **24** 18655
[28] Zhuang L *et al* 2015 *Optica* **2** 854
[29] Liu Y *et al* 2016 *Opt. Lett.* **41** 5078
[30] Liao S *et al* 2014 *Opt. Express* **22** 31993
[31] Cheng C and Rebeiz G M 2012 *IEEE Trans. Microw. Theory Tech.* **8** 2431
[32] Psychogiou D *et al* 2016 *IEEE Trans. Circuits Syst.* II **63** 79
[33] Ko C, Tran A and Rebeiz G M 2015 *IEEE Trans. Microw. Theory Tech.* **63** 1854
[34] Dupuis N *et al* 2015 *J. Lightwave Technol.* **33** 3597
[35] Rasras M S *et al* 2009 *J. Lightwave Technol.* **27** 2105